Adsorption of methane and carbon dioxide by water-saturated clay minerals and clay rocks

Denys Grekov, Jean-Charles Robinet, Bernd Grambow

Adsorption of methane and carbon dioxide by water-saturated clay minerals and clay rocks

Denys I. Grekov,[a]* Jean-Charles Robinet,[b] Bernd Grambow[c]

[a] IMT Atlantique, GEPEA, UMR CNRS 6144, F-44307 Nantes, France

[b]Andra, R&D Division, Transfer Migration Group, 92298 Châtenay-Malabry, France

[c]SUBATECH, (IMT Atlantique, CNRS -IN2P3, Université de Nantes), F-44307 Nantes, France

Corresponding author: denys.grekov@imt-atlantique.fr

Keywords: Adsorption, clay rock, saturation, CH_4, CO_2.

Abstract

Understanding the effects of water on gas adsorption in geological media is of high importance in order to efficiently control numerous subsurface engineering process operating at gas/rock interfaces. Due to preferential interaction with clay surfaces, water fills their porous body, greatly reducing CH_4 and CO_2 adsorption capacity. In order to quantitatively describe CH_4 and CO_2 adsorption by hydrated clay minerals, this work proposes to rely on the mechanism of gas uptake by dissolution in pre-adsorbed pore water. This approach was employed to characterise water-saturated porous media of increasing complexity: mesoporous silica SBA-15 and silica gel with different pore sizes and geometry, isolated illite and montmorillonite and natural clay-rich rock (the Callovo-Oxfordian formation – COx, France) in powdered and crushed states. It was found that the solubility in water can reliably explain the CO_2 uptakes by hydrated pore systems regardless of their nature as well as the CH_4 uptakes, but only for solids with large mesopores and montmorillonite mineral. A so called "adsorption enhanced gas uptake in pore water" for CH_4, exceeding its solubility in bulk water by a factor of 5-8, was observed for the systems with narrow pore sizes, highlighting the impact of surface energy on gas uptake and the occurrence of the interaction of weakly-soluble methane with the surface, promoting its uptake in comparison to pure dissolution.

1. Introduction

Many geological gas reservoirs are natural subsurface rock formations with high surface area/void volume ratio, so they may enclose a significant part of trapped CH_4, CO_2 and other gases in adsorbed state. Clays are major mineral components of gas reservoirs, determining their porous structure and transport properties (Harrington and Horseman, 1999; Gensterblum et al., 2015). Multiscale/multiphysics understanding of these geological media is of prime importance to efficiently adapt deep engineering process, such as shale gas extraction, natural hydrogen recovery, geological gas storage or CO_2 sequestration (Benson and Cole, 2008; Busch et al., 2008; Plaat, 2009; Schaef et al., 2014; Cooper et al., 2016). Gas migration in clay-rocks are also deterministic for operation as well as safety assessments of geological radioactive waste disposal sites (Marschall et al., 2005). For instance, in these systems, at geological time scale, in addition to the release of gaseous hydrogen due to anaerobic corrosion of steel and reactive metals and to a much smaller degree due to water radiolysis, a significant part of gaseous organic degradation products or of ^{14}C-containing species may exist, depending on redox and pH conditions, in form of CH_4 or CO_2 (Grambow, 2016). Gas production processes are normally slow but it is possible that gas generation is faster than gas dissolution and migration through the engineered barrier components and the host rock, leading to desaturation of water saturated rock and diphasic gas flow in the repository and its near field.

Realistic assessment of the capacity of geological gas reservoirs and the migration of gas through natural barriers should rely not only on textural or geomechanical properties and composition of rock, but it should also take into account the effect of water which is omnipresent at near-saturation in many geological systems.

The mechanism of gas adsorption in presence of water is complex and strongly depends on the type of porous media, the amount of water it contains, pressure and

69 temperature conditions. Since water is a polar molecule, it strongly and preferentially interacts
70 with charged surface species, such as cations or hydroxyl groups, greatly reducing the number
71 of available sites for the adsorption of other gases and vapours at the surface or inside
72 micropores. For oxide systems, bearing significant amounts of polar surface species, the
73 completion of pre-adsorbed water layers occurs at low relative humidity, greatly reducing the
74 adsorption of CH_4 and CO_2 due to a "competition" effect (Kamimura and Endo, 2015;
75 Tsujiguchi et al., 2016; AbdulKareem et al., 2018; Wang et al., 2020; Zhao et al., 2020).
76 Under the same conditions, carbonaceous solids adsorb much lower amounts of water with
77 the respect to their surface area, so that the process of CH_4 and CO_2 adsorption are almost
78 unaffected by the effects of moisture at low and moderate relative humidity (Billemont et al.,
79 2011, 2013; Tsujiguchi et al., 2016). In several specific cases, the presence of small amounts
80 of water in the solid (at the initial stages of hydration) can albeit promote the adsorption of
81 gases, due to the opening of the interlayer porosity in case of clays (D. I. Grekov et al., 2020;
82 Ziemiański et al., 2020) or modification of the energetics or the availability of adsorption sites
83 in case of amphiphilic MOFs (Wang et al., 2017; Benoit et al., 2018) upon water uptake. For
84 example, in case of smectite clays, the interlayer spaces are usually inaccessible for the
85 incorporation of gases under fully-dehydrated conditions. At initial stages of water adsorption,
86 the coordination of H_2O molecules to the charge-balancing cations results in expansion of the
87 interlayer spaces, which makes them accessible for the diffusion of gases (Loring et al., 2012;
88 Rother et al., 2013; Bowers et al., 2017, 2018, 2019; Loganathan et al., 2017, 2018; Schaef et
89 al., 2017). It greatly increases CH_4 and CO_2 uptakes in comparison to completely dehydrated
90 smectite clays, featuring the collapsed state of the interlayers and adsorbing gases mainly at
91 external particle surfaces (Liu et al., 2013; Liang et al., 2016; Hwang and Pini, 2019; D. I.
92 Grekov et al., 2020; Du et al., 2020; Ziemiański et al., 2020).

Saturation with water of any porous media and of clay minerals in particular, usually results in lower capacities for gas uptake (except, perhaps the cases of gas hydrate formation) in comparison to fully dehydrated counterparts (Merkel et al., 2015a, 2015b; Li et al., 2016; Feng et al., 2018a). A number of studies carried out on shales, clay rocks, isolated clay minerals and coals, both in their dry state and equilibrated under different relative humidity (RH) conditions, revealed a progressive and usually linear decrease in CH_4 and CO_2 adsorption with increasing moisture content, until a threshold value, usually reached above 70% of RH. This is probably due to the filling of the smallest pores by water and hence the loss of an interconnected gas phase, strongly limiting the accessibility of gas to the overall pore network (Gensterblum et al., 2013; Merkel et al., 2015a, 2015b, 2016; Kadoura et al., 2016; Li et al., 2016; Feng et al., 2018b, 2018a). For pure clay phases, it is more related to the accessibility of surface due to presence of adsorbed water molecules. While several attempts were made to quantitatively interpret the reported trends, predictive models of gas adsorption in hydrated clay systems remain highly uncertain (Li et al., 2016; Feng et al., 2018b; Han et al., 2021). The uncertainty mainly comes from complex issues of the behaviour of gases in water confined inside nm-sized interparticle and charged interlayer (in case of smectites) pores, strong heterogeneity of clay minerals and lack of the understanding of gas transport and porous structure of hydrated geological systems (Holmboe et al., 2012; Massat et al., 2016).

According to recent experimental and molecular dynamics works, the uptakes of dissolved gases in liquid-filled nm-sized pores (S), are usually greater than given by gas solubility in bulk liquids ($S°$) under the same (P, T) conditions. The observed phenomenon, which refers to the effect of surface energy, was often termed “oversolubility” (Luzar and Bratko, 2005; Bratko and Luzar, 2008; Pera-Titus et al., 2009; Rakotovao et al., 2010; Clauzier et al., 2012; Ho et al., 2015; Coasne and Farrusseng, 2019; Liu et al., 2020). It is a complex phenomenon supposed to be due to the layering of water (solvent) molecules in the

vicinity of the charged surface of pores of the solid, promoting the organization of the dissolved gas molecules and/or their interaction with pore wall indicating adsorption phenomena. In the present work the term "adsorption-enhanced gas uptake in pore water" is employed instead of "oversolubility". The apparent solubility enhancement factor $s \sim S/S°$, was found to decrease with the increasing $S°$ and to be higher for non-polar solvents (5-30) in comparison to polar ones, such as water, alcohols or halogenated hydrocarbons (1 – 7) (Pera-Titus et al., 2009; Rakotovao et al., 2010; Clauzier et al., 2012). Textural properties of porous solids figure among key factors influencing the observed solubility enhancement factor – $S/S°$. For instance, systems with high surface area/pore volume ratio, characteristic for narrow pores (typically with sizes ranging between 3 and 6 nm) seem to offer the highest observed $S/S°$ ratios, as compared to larger pore sizes.

The main objective of the present study was to experimentally verify to which extent the solubility in bulk water can explain CH_4 and CO_2 uptake by clay minerals under water-saturation conditions (Gadikota et al., 2017). To address this question, adsorption isotherms were measured for a series of porous media of increasing complexity: model mesoporous silica, pure clay phases (montmorillonite and illite, with interlayers, which are either accessible or inaccessible for water/gases) and clay –rock samples, all equilibrated under controlled (97%) RH conditions. Measured adsorption capacities were calculated with the respect to the amounts of water contained in samples and directly compared to the solubility of CH_4 and CO_2 in bulk water under the same (P, T) conditions.

2. Materials and methods

2.1. Clays and porous silica

Davisil silica gel and SBA-15 mesoporous silica were supplied by Sigma Aldrich. Pure-phase montmorillonite (referred as Mt) was obtained from Na-bentonite Kunipia F, received from Kunimine industries. Mt of Kunipia F mainly features the substitutions in octahedral layer, with the structural formula $(X(I)_{0.44})[Al_{1.56}Mg_{0.305}Fe_{0.1}][Si_{3.95}Al_{0.05}]O_{10}(OH)_2$, where the principal cationic species in the exchangeable domain (X(I)) is Na^+ (Suzuki et al., 2004). After dispersion in deionized water (5 g/l) the <2 µm fraction was extracted by centrifugation at 1000 rpm (170 g) and exchanged with Na by 24 h contact with 0.2 mol/l NaCl solution, 6 cycles of centrifugation at 20000 rpm (44800 g) and washing in deionized water, final washing in methanol and drying of suspension at 50°C. Illite du Puy (I) was received from BRGM (Orléans, France) in a Na-exchanged form (Gaboreau et al., 2016). After the dispersion in demineralized water under ultrasound (30 min), it was further purified from quartz by an elutriation procedure and exchanged with Na by following the same protocol as for montmorillonite. In contrast to Mt, I presents the substitutions in both tetrahedral and octahedral layers and its structural formula is : $(X(I)_{0.12}Ca_{0.01}Na_{0.01}K_{0.53})[Si_{3.55}Al_{0.45}][Al_{1.27}Fe(III)_{0.36}Mg_{0.44}]O_{10}(OH)_2$ (Bardot, 1998). According to (Bardot, 1998; Bradbury and Baeyens, 2009; Gaboreau et al., 2016), illite du Puy contain 5-10% of smectite phases. The core samples of a natural clay-rock used come from the Callovo-Oxfordian (COx) mudstones, East of Paris basin, France (Gaucher et al., 2004). COx clay rock is mainly composed of clay minerals such as illite (I) and interstratified illite/smectite (I/S) phases, carbonates (C) and tectosilicates (T). Smectite fraction is mainly dominated by montmorillonite. Several depths were selected in order to analyse various clay fractions and I/S ratios. The mineralogical characteristics of the samples were reported in earlier works (Grekov et al., 2019, 2021; D. Grekov et al., 2020) and are summarized in Table 1.

Table 1. Simplified composition of clay samples.

Clay sample	Tectosilicates, %	Carbonates, %	Clay fraction	
			Content %	Simplified composition
Montmorillonite*	-	-	>95	Montmorillonite:
Illite du Puy	-	-	>95	Illite
COx-EST 48599 (-508,3 m)	20-30	25-35	40-50	Illite: 75-80% Smectite: 20-25%
COx-EST 48601 (-466 m)	20-30	25-30	40-50	Illite: 60-70% Smectite: 30-40%

166 * extracted from bentonite Kunipia F

167 Clay samples were ground manually and sieved to collect a size fraction <100 µm. All
168 the material was ground until it was smaller than 100 µm. Some COx clay rocks were crushed
169 to the size of ~5-15 mm. Crushed and powdered samples are labelled "C" and "P"
170 respectively. A part of prepared clays together with mesoporous silica were equilibrated at ≈
171 97% of RH at 20°C, inside a desiccator over saturated K_2SO_4 solution during 1 month.

172 *2.2. CH_4 and CO_2 adsorption measurements*

173 A manometric method was used for measurement of CH_4 and CO_2 adsorption
174 isotherms at 20°C and pressures ranging between P_{atm} and 8 MPa, following the methodology
175 reported earlier (D. I. Grekov et al., 2020; Grekov et al., 2021). The principle of the
176 experimental setup is described in *Electronic Supplementary Information.* Samples for gas
177 adsorption measurement are usually outgassed under dynamic vacuum and heating. However,
178 in the present study, in order to preserve the hydrated structure of humidity-equilibrated
179 solids, after being packed in measurement cell, powdered or ground samples of 5-8 g were
180 purged with working gases 3 times and briefly (less than 30 s) evacuated to about 0.1 bar, to
181 stay above water vapour saturation pressure at 20°C for isotherm measurement. This protocol
182 was validated by comparing hydrated sample weights before and after isotherm measurement;
183 the weight variation did not exceed 1%. Note, that under given pressure conditions (up to 9
184 MPa), some of the H_2O molecules could be replaced by CO_2 or CH_4, thus being lost from the

sample due to their transfer to the gas phase. Also, the observed weight loss could partially be explained by the sample's loss, due to sticking of the moist solid to the wall of adsorption measurement cell. In order to minimize an error propagation, the isotherms for hydrated solids were measured within two runs (of 3-4 points) on the same sample. CH_4 adsorption was measured before CO_2.

Isotherms were also collected for dehydrated clays and silica; those were outgassed at 170°C for 24 h in an oven, rapidly transferred to the sample cell and further outgassed for another 24 h under dynamic vacuum, as reported in the previous works (D. I. Grekov et al., 2020; Grekov et al., 2021). The dead volumes V_d of the sample holder, including free space in the sample cell, inter-particle voids and micro/mesoporous volume, were determined for dry and humidity-saturated solids by He expansion at different pressures (2-8 bar) within 4 runs. Measurement of the V_d at pressures above the atmospheric pressure allows to mitigate the error induced by H_2O vapour partial pressure in case of water-saturated samples.

2.3. Thermo-gravimetric analysis (TGA)

The measurements of water content in humidity-equilibrated solids were carried out with Setaram TG-DSC 111 thermo-gravimetric analyser. 5-20 mg of hydrated solid were heated in quartz crucibles from ambient temperature up to 800°C under 20 ml/l of He flow. Temperature-induced weight variations were corrected by subtracting the TGA curves acquired for an empty crucible.

2.4. Textural analysis

External specific surface areas were determined from N_2 adsorption isotherms at -196°C using the BET method by following the IUPAC recommendations (Thommes et al., 2015). The total porous volume was calculated from the amount of N_2 adsorbed at 0.95 $p/p°$. Pore sizes were determined from adsorption isotherms by applying the NLDFT (non-local density functional theory) model with the kernel for cylindrical pore for oxide surface

(Maddox et al., 1997; Occelli et al., 2002, 2003). Adsorbed N_2 molecule cross section area at -196°C used in the calculations was 0.162 nm^2.

Nitrogen adsorption isotherms were collected at relative pressure ranging between 10^{-5} and 1 using 3Flex automated static manometric adsorption analyser from Micromeritics. Before isotherm measurement, all samples were outgassed under dynamic secondary vacuum at 150°C until residual pressure stabilization for at least 24 h. The volumes of cells unoccupied with the sample were determined at ambient temperature and at -196°C by helium expansion.

3. Results and discussion

3.1. CH_4 and CO_2 adsorption by model porous silica

Among large number of works on the effects of moisture on gas physisorption, only a few studies refer to the systems at complete saturation with water at near-ambient temperature or above (Liu et al., 2013, 2020; Merkel et al., 2015a, 2016; Feng et al., 2018b). Thereby, in order to better understand the behaviour of CH_4 and CO_2 in nanoconfined water, gas adsorption measurements on model porous systems saturated with water are required. Mesoporous silica SBA-15 and silica gel are suitable materials for such assays.

N_2 adsorption isotherms of SBA-15 and silica gel, shown in Fig. 1 (a), featured shape IV(a) according to the IUPAC classification (Thommes et al., 2015), confirming their mesoporous character, as usually reported for such materials (Thielemann et al., 2011; Cychosz et al., 2017; Kutarov and Schieferstein, 2019). For SBA-15, H1-type hysteresis between adsorption and desorption isotherms signified regular narrowly-distributed cylindrical pores, consistent with the synthesis route of this material. Large H2(b) hysteresis loop for silica gel, was indicative of ink-bottle pore geometry with the distribution of sizes of

234 both, pore bodies and pore openings. This conclusion was supported by the results of pore
235 size distribution analysis using the NLDFT method. Both mesoporous silica featured close
236 values of the BET surface area (550 and 480 m^2/g for SBA-15 and silica gel respectively) but
237 significantly differed in terms of pore volumes (0.42 and 0.87 cm^3/g respectively) and pore
238 size distribution (6-8 and 6-20 nm respectively), Table 2. Thermogravimetric curves of
239 humidity-saturated materials are represented in Fig. 1 (b). Weight loss of 27 and 47% before
240 150°C for SBA-15 and silica gel, were assigned to the evaporation of capillary-condensed
241 water and corresponded to 0.37 g/g and 0.88 g/g of water content with the respect of dry
242 material. A good agreement between these values and mesopore volumes determined from N_2
243 adsorption, suggested a complete filling of pores with water at 97% of RH. The same
244 conclusion was driven from a direct analysis of H_2O adsorption isotherms for such systems
245 (Lin et al., 2018; Centineo et al., 2019).

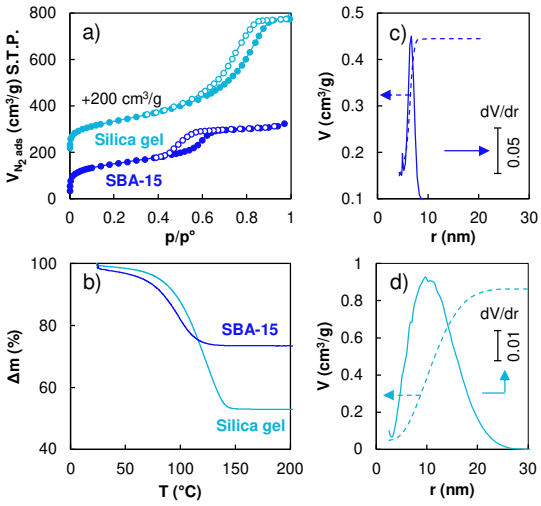

246

247 **Fig. 1.** (a) N_2 adsorption (filled symbols) and desorption (empty symbols) isotherms for SBA-
248 15 (dark blue) and silica gel (ocean blue), (b) TGA curves (of humidity-saturated samples)
249 and pore size distribution obtained using NLDFT for (c) SBA-15 and (d) silica gel.

250 CH_4 and CO_2 adsorption isotherms measured for both materials in dry and humidity-
251 saturated states are represented in Fig. 2. The shape of methane adsorption isotherms for

dehydrated silica is consistent with a monolayer formation on the pore surface. Higher adsorption capacity for SBA-15 in comparison to silica gel was due to its higher BET surface area. The adsorption isotherms of CO_2 featured a more complex shape with a progressively ascending component in the higher pressure range instead of a plateau, which could be due to polymolecular adsorption of subcritical at 20°C CO_2. Both materials lost 80-90% of adsorption capacity under water-saturation conditions, which agrees with commonly observed trend (Kamimura and Endo, 2015; Merkel et al., 2015a, 2015b, 2016; Li et al., 2016; Feng et al., 2018a). Isotherms featured a linear shape. In order to verify to which extent one can consider the solubility of gases in pore water to explain gas uptakes, the adsorbed amounts of CH_4 and CO_2 were calculated with the respect of water content in materials and plotted against pressure, together with the solubility of these gases in bulk water at 20°C (Diamond and Akinfiev, 2003; Duan and Mao, 2006), Fig. 2 (c).

Table 2. BET surface area, pore volume (from N_2 adsorption isotherm) and water content at 97% of RH at 20°C of studied samples.

Material	S_{BET} (m^2/g)	$V_{p\ tot}$ (cm^3/g)	m_{H_2O} ($g/g_{dry\ solid}$)
SBA-15	550	0.42	0.37
Silica gel	480	0.87	0.88
I	131	0.27	0.27
Mt	35	0.03	0.34
EST48599 (P)	38	0.05	0.06
EST48599 (C)	36	0.05	0.07
EST48601 (P)	31	0.03	0.05
EST48601 (C)	30	0.03	0.07

266 According to the results in Fig. 2(c), in pressure range investigated herein (0.1-8
267 MPa), methane featured almost 10 times higher apparent solubility in water confined in SBA-
268 15 mesopores in comparison to the bulk water. The same order of magnitude of the
269 "oversolubility" was reported for similar systems studied earlier (Pera-Titus et al., 2009;
270 Rakotovao et al., 2010; Clauzier et al., 2012). Regardless of the origins of enhanced gas
271 uptake in nano-confined water as compared to bulk water (higher solubility of gas in ordered
272 liquid adjacent to the surface or "attractive" interaction of the dissolved gas molecules with
273 the pore wall, Fig. 2(d)), the surface area/pore volume ratio of the porous solid is the key
274 factor controlling the process. Thus, in case of silica gel, which in contrast to SBA-15
275 featured lower surface area/pore volume ratio (550 m^2/cm^3 *vs.* 1310 m^2/cm^3) due to larger
276 pore sizes, the measured amounts of adsorbed methane exceeded methane solubility in bulk
277 water by only a factor of 1.8.

278 The same trend was observed for carbon dioxide, however adsorption-enhanced gas
279 uptake in pore water was less significant and the adsorbed amounts only slightly exceeded the
280 solubility of CO_2 in bulk water (factor of 1.3 for silica gel and 2.7 for SBA-15, Fig. 2 (c)).

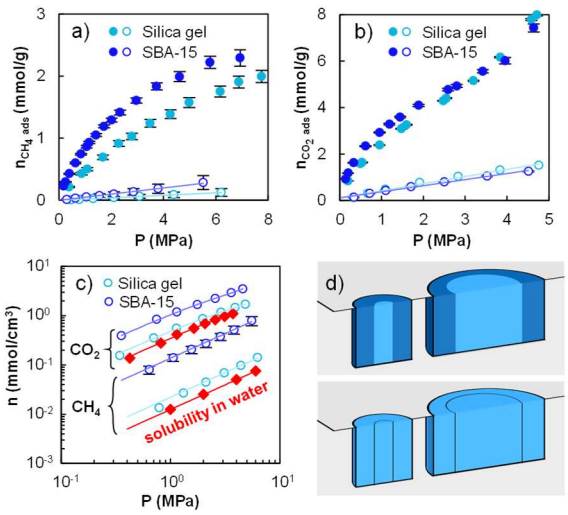

281

282 **Fig. 2.** CH_4 (a) and CO_2 (b) adsorption isotherms for SBA-15 (dark blue) and silica gel (ocean
283 blue) under dehydrated (filled symbols) and water-saturated at 97% of RH (open symbols)

284 states, (c) comparison of the solubility of CH_4 and CO_2 in water confined inside SBA-15 and
285 silica gel pores and in bulk water (red lines) (Diamond and Akinfiev, 2003; Duan and Mao,
286 2006), (d) schematic illustration of the distribution of water states in nanopores filled with
287 water: top – strongly-confined ordered pore water (dark blue) and weakly-confined bulk-like
288 water (light blue), bottom – area of adsorption-enhanced interaction of dissolved gas
289 molecules with pore wall.

290 Regarding linear domains of the isotherms, the uptake of CO_2 by dehydrated solids
291 exceeded the uptake of CH_4 by a factor of 3-5, while in case of the dissolution of these gases
292 in bulk water, this ratio was as high as 30 (in favour of CO_2, respective solubilises are $3.4 \cdot 10^{-5}$
293 and $1.25 \cdot 10^{-6}$ $mol \cdot cm^{-3} \cdot bar^{-1}$ at 20°C) (Diamond and Akinfiev, 2003; Duan and Mao, 2006).
294 Thereby, for the weakly soluble methane the interaction of the molecules with pore wall of
295 water-saturated silica promotes the uptake, and for CO_2 the process is mainly controlled by
296 dissolution. This conclusion is fully in line with the trends reported in the literature (Luzar
297 and Bratko, 2005; Bratko and Luzar, 2008; Pera-Titus et al., 2009; Rakotovao et al., 2010;
298 Clauzier et al., 2012; Ho et al., 2015; Coasne and Farrusseng, 2019; Liu et al., 2020).

299 *3.2. CH_4 and CO_2 adsorption by clay minerals and clay rocks*

300 Illite and smectite phases as well as interstratified illite/smectite are frequently the
301 principal constituents of many clay-rich rock formations, such as argillite. In contrast to illite,
302 smectites have interlayers allowing exchange with the pore solutions. The low porosity of
303 these formations is mainly associated to their clay fraction, so illite and smectite phases
304 spatial distribution determines textural and fluid transport properties of rocks (Yven and
305 Sammartino, 2007; Robinet et al., 2015; Song et al., 2015; Gaboreau et al., 2016). Various
306 isolated phyllosilicate minerals, including mentioned clay phases, were extensively studied by
307 high-pressure gas adsorption measurements (Giesting et al., 2012; Liu et al., 2013; Pini, 2014;
308 Rexer et al., 2014; Pozo et al., 2017; Hwang and Pini, 2019; Hwang et al., 2019). At constant

309 temperature, pressure and water content, the amounts of methane and carbon dioxide
310 adsorbed by clay minerals depend on their specific surface area and on the accessibility of the
311 interlayer spaces in case of smectites (D. I. Grekov et al., 2020; Ziemiański et al., 2020;
312 Hwang and Pini, 2021). The affinity of gas molecules to the clay surfaces correlates with the
313 nature of exposed charge-balancing cations, structural charges and the shape of clay particles
314 (Melnitchenko et al., 2000; Loganathan et al., 2020; Grekov et al., 2021).

315 While the sorption of CO_2 and CH_4 in dry state is mainly controlled by available
316 surface area and remains rather clear concept, sorption of CO_2, accompanied by dissolution in
317 pore water needs to be exposed to the same chemical constraints as any dissolved CO_2:
318 formation of $CO_2(aq)$, H_2CO_3, HCO_3^- and CO_3^{2-} species, depending on pH conditions and
319 CO_2 partial pressure. In order to assess the impact of clay rock pore water composition on
320 CO_2 solubility and to account for the non-linear relation between CO_2 partial pressure and
321 dissolved CO_2, geochemical modelling was conducted, using PHREEQC code (Parkhurst and
322 Appelo, 2013). The pore water model of the Callovo-Oxfordian (Gaucher et al., 2006) clay
323 rock was used to assess the impact of increased CO_2 pressure on pore water pH, ionic strength
324 and CO_2 solubility in typical clay rock. This model accounts for mineral (calcite, illite,
325 dolomite, quartz, pyrite, celestine, Fe chlorite) and ion exchange equilibria at 25°C. The initial
326 equilibrium partial pressure of CO_2 controlled by the mineral phase equilibria was calculated
327 to be 10^{-2} bar, the pH was 7.21 and the ionic strength 0.11 $mol \cdot kg^{-1}$. Under these conditions
328 80% of the total dissolved CO_2 exists in form of HCO_3^-, 10% as CO_3^{2-} and only 10% as
329 $CO_2(aq)$. At an imposed pressure of either 1 or 10 bar $CO_2(g)$ respectively, the pore water pH
330 decreases to 6.06 or 5.48 and the total dissolved CO_2 becomes to 55% or 82% $CO_2(aq)$,
331 approaching linearity between CO_2 pressure and dissolved CO_2 at high pressures. Caused by
332 acidification of pore water and mineral dissolution, the ionic strength rises to either 0.14 or
333 0.18 $mol \cdot kg^{-1}$. However, the impact of slight ionic strength variation on gas solubility is low,

so its effect is not taken into account. The results of simulation are shown in Fig. S1. The prevalence of dissolved molecular CO_2 at elevated CO_2 pressures was also shown experimentally (Peng et al., 2013).

CH_4 and CO_2 adsorption isotherms for pure-phase illite and montmorillonite are represented in Fig. 3 (a), (b), (e), (f). Isotherms featured the same shape as in case of model mesoporous silica and the measured adsorption capacities under dehydrated conditions were in a good agreement with the results for similar montmorillonite and illite clays, with the respect to their BET surface areas (Ross and Marc Bustin, 2009; Liu et al., 2013; Jeon et al., 2014; Liang et al., 2016; Hwang and Pini, 2019; Hwang et al., 2019).

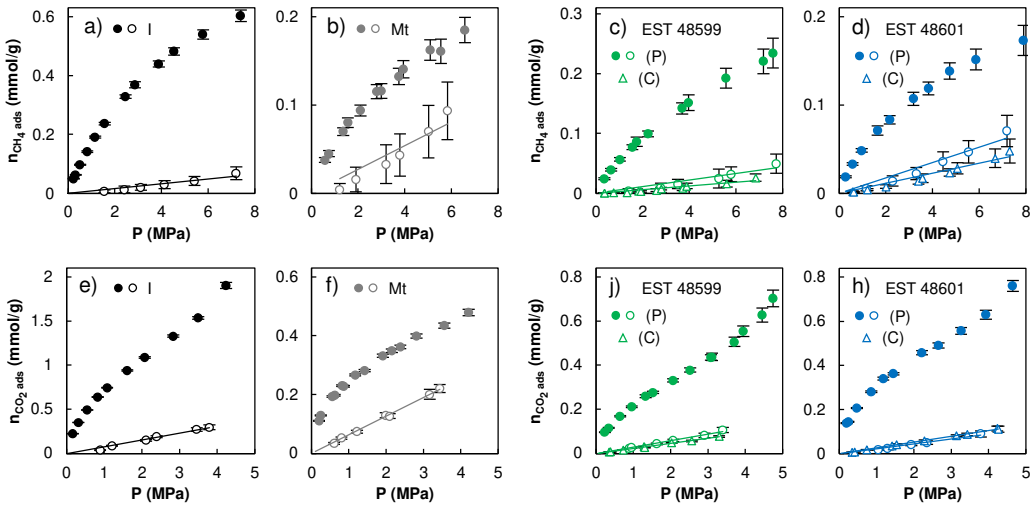

Fig. 3. Adsorption isotherms for CH_4 (figures a – d) and for CO_2 (figures e – h) for single-phase illite du Puy - I (a), (e) and montmorillonite - Mt (b), (f) clays and for Callovo-Oxfordian clay rock samples EST 48599 (c), (j) and EST 48601 (d), (h) under dehydrated (filled symbols) and humidity-saturated (empty symbols) states. Triangles and circles correspond to crushed (C) and powdered (P) samples respectively. Gas adsorption isotherms by water-saturated clays are approximated by a line.

As expected, gas adsorption capacities dropped for both clay minerals under water-saturation conditions as compared to the dehydrated state. Gas adsorption isotherms by

352 hydrated solids had rather linear shape. Montmorillonite loses by hydration about 50% of
353 adsorption capacity for both gases, while illite – 80% and 90% for CO_2 and CH_4 respectively.

354 TGA curves allowed discerning two weight loss domains for hydrated clay minerals:
355 before 150°C, assigned to the evaporation of physisorbed water and above 500°C, due to the
356 dehydroxylation of the phyllosilicate structure, Fig. S3. Regarding the amounts of adsorbed
357 CH_4 and CO_2 per total volume of water physisorbed at saturation, determined from the results
358 of TGA (without distinguishing between interlayer and pore water in case of montmorillonite)
359 (Ferrage et al., 2010; Ferrage, 2016; Grekov et al., 2019) one can realise that the solubility of
360 gases in physisorbed water can reliably explain gas uptakes by both clay minerals, Fig. 4 (a)
361 and (b). For I, which similarly to silica gel, features large mesopores (the closing of hysteresis
362 loop between nitrogen adsorption/desorption isotherms at $p/p° \sim 0.8$, Fig. S2), the absence of
363 significant enhancement of CH_4 and CO_2 uptakes in comparison to the solubility of these
364 gases in bulk water, could be explained by weak confinement effect of the capillary water due
365 to low surface area/pore volume ratio, typical for large pore sizes. On the other hand, the
366 origins of the same behaviour in case of montmorillonite were not entirely clear. Indeed,
367 under saturation conditions, Mt feature a significant fraction (about 50%) (Ferrage et al.,
368 2010; Grekov et al., 2019) of strongly confined interlayer water and according to atomistic
369 simulation works, are able to incorporate gases in the interlayer spaces (Gadikota et al., 2017).
370 Considering a high confinement of the interlayer water, composed of 2-3 layers of organized
371 H_2O molecules, in view of the foregoing, one should expect adsorption enhanced gas uptake
372 in interlayer water in comparison to the solubility in bulk water.

373 Taking into account the prevalence of molecular form of dissolved CO_2 over HCO_3^-
374 and CO_3^{2-} in clay pore water at pCO_2 pressures > 1 bar and the impossibility of the two latter
375 species to enter the interlayers at elevated carbon dioxide pressure, only CO_2 (major species
376 of dissolved carbon dioxide) can enter the interlayer space of hydrated smectites (Loring et

al., 2012, 2014; Schaef et al., 2012), depending on RH and possibly the type of interlayer cations. Thus, the observed picture for montmorillonite may signify the existence of two antagonistic effects upon gas uptake: on one side, the confinement of CH_4 and CO_2 molecules in hydrated interlayer space (Myshakin et al., 2013; Bowers et al., 2017; Gadikota et al., 2017) promoting the apparent adsorption-enhanced gas uptake, and on the other side, a high ionic force due to the presence of charge-balancing cations, suppressing gas uptake (Li et al., 2020). As shown by atomistic simulations, an increase of hydrated smectite interlayer distance results in a decrease of CO_2 solubility in the interlayer water (Botan et al., 2010) making it close to that in a bulk water under saturation conditions. According to (Botan et al., 2010; Gadikota et al., 2017), CO_2 uptake in the interlayer water (2W and 3W states) exceeds the solubility in bulk water by only a factor of 2-4.

Fig. 3 (c), (d), (j), (h) summarizes CH_4 and CO_2 adsorption isotherms for dry and humidity-saturated COx clay rock samples. It was illustrated that several properties of clay rocks, such as cation exchange capacity or retention of dissolved chemical species, related to phyllosilicate layer charge and illite/smectite ratio, can be described in “bottom-up” approach relying on the properties of pure-phase illite and montmorillonite (Tournassat et al., 2009). This concept cannot directly be employed today to describe the tendencies in gas physisorption, which, primarily depend on the textural properties of clay minerals. Even though, the impact of kerogens and other organic matter contents on CH_4 sorption might need to be considered as well.

Due to close values of the BET surface area, Table 2, humidity-saturated powdered and crushed argillite samples adsorbed similar quantities of CH_4 and CO_2. This observation was supported by the conclusion of the work (Robinet et al., 2012), which showed that COx size fraction < 100 µm is representative of the bulk rock microstructure.

Within experimental error CO_2 uptakes by humidity-saturated COx clay rock (in terms of mmol/cm^3 of pre-adsorbed water) were close to CO_2 solubility in bulk water, Fig. 4. The measured volumetric uptakes did not significantly differ neither for the clay rock composition (Table 2) nor for the granulometry of the samples. It is worthy to be noticed that since at low pressure the CO_2 uptake in alkaline pore water is dominated by the formation HCO_3^- species, one may expect for COx clay rocks a higher CO_2 adsorption-enhanced uptake in the interlayer water at sub-atmospheric pressure range in comparison to a high pressure. This could not be concluded from the measurements performed far above 1 atm in the frame of this work. The data reported in Fig. 4 is also summarized in Table 3.

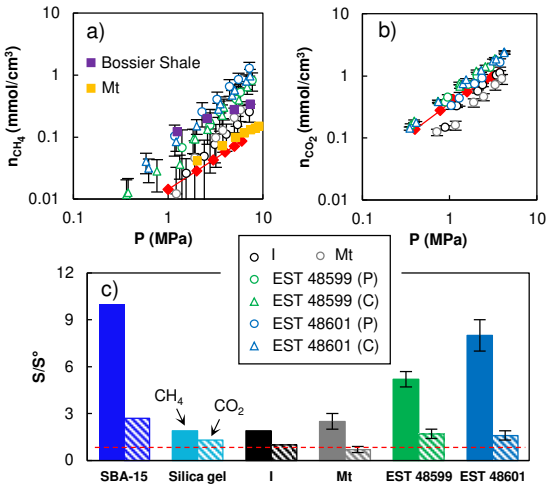

Fig. 4. Comparison of the solubility of CH_4 (a) and CO_2 (b) in water confined in pores of clay minerals and in bulk water (red symbols) (Diamond and Akinfiev, 2003; Duan and Mao, 2006). (c) Comparison of CH_4 and CO_2 adsorption-enhanced gas uptake in pore water (S) with the respect to their solubility in bulk water (S°) at 20 °C ($1.25 \cdot 10^{-6}$ and $3.4 \cdot 10^{-5}$ mol·cm^{-3}·bar^{-1} CH_4 and CO_2 respectively) for different porous solids. Violet and yellow squares correspond to CH_4 adsorption isotherms by water-saturated Bossier shale and montmorillonite from works of (Merkel et al., 2015a) and (Li et al., 2016).

418 On the other hand, volumetric CH_4 uptakes by COx clay rock samples exceeded CH_4
419 solubility in bulk water by a factor of 5-8, which could be due to the effect of confinement in
420 nanosized pores, by analogy with SBA-15. Combining the inputs from 3D FIB-SEM image
421 reconstruction, mercury intrusion porosimetry, N_2 adsorption and recently from
422 thermoporometry applied to water-saturated clays, it was reported that pores in the Callovo-
423 Oxfordian clay rock typically range from the order of several nm to several dozens of nm
424 (Yven and Sammartino, 2007; Song et al., 2015; Gaboreau et al., 2016; Grekov et al., 2019).
425 Such narrow pore sizes in clay-rocks result from chemo-mechanical constrains acquired
426 during the diagenesis. They mainly originate from the mechanical compaction due to the
427 lithostatic pressure and the precipitation of nm-sized mineral grains within the porosity. In
428 case of isolated Mt, desagregated by ultrasound treatment in aqueous media during
429 purification procedure, these constrains do not exist. Hence, upon swelling in moist
430 atmosphere, the inter-granular pores size can be larger in comparison to COx clay rock. As a
431 consequence, purified clay minerals and raw clay rock samples exhibited different pore sizes
432 under the saturation conditions, so the enhancement of methane uptake in comparison to its
433 solubility in bulk water was contrasted for these clay systems. Interestingly, EST 48601
434 sample featured slightly higher methane uptake in pore water than EST 48599 sample, which
435 could be explained by narrower pores as suggested by its lower BET surface area / pore
436 volume ratio (Table 2).

437 **Table 3.** The solubility of CH_4 and CO_2 in pore water of humidity-saturated solids with the
438 respect to their solubility in bulk water ($S/S°$) according to (Diamond and Akinfiev, 2003;
439 Duan and Mao, 2006.

	SBA-15	Silica gel	I	Mt	EST 48599	EST 48601
CH_4	10	1.9	1.9	2.5±0.5	5.2±0.5	8±1
CO_2	2.7	1.3	1	0.7±0.2	1.7±0.3	1.6±0.3

440

As demonstrated for shales of different maturity, CH_4 and CO_2 adsorption capacities positively correlate with the content of organic carbon (kerogen) in these systems (Ross and Marc Bustin, 2009; Gensterblum et al., 2013; Merkel et al., 2015a, 2015b; Hu and Mischo, 2020; Klewiah et al., 2020; Li et al., 2021). Due to hydrophobic character of kerogen, contented up to more than 20% in several shales, organic-rich formations adsorb less water than clay rocks, under saturation conditions, so their surfaces and pores remain more accessible for the adsorption of gases, presaging them with higher adsorption capacities than clay rock characterised by a low content of organic matter (Merkel et al., 2015a, 2016). It is thus important to exclude the effect of organic matter, to properly adapt the term of adsorption-enhanced gas uptake in pore water for raw natural clay rocks. In case of COx clay-rock, containing less than 2% of organic carbon (Gaucher et al., 2004), the effect of kerogen on CH_4 and CO_2 adsorption should not be significant (Merkel et al., 2015a, 2016). Methane adsorption data for humidity-saturated pure-phase montmorillonite (Li et al., 2016) and low-organic carbon Bossier shale (Merkel et al., 2015a) (content of kerogen close to that in COx) perfectly agreed with the trend reported in this study, Fig. 4 (a), indicating that the observed effect is not an artefact but a real consequence of adsorption-enhanced gas uptake in pore water. Consequently, in natural clay rock formations, the results from this study suggested that CH_4 and CO_2 adsorption-enhanced uptakes in pore water can be strongly contrasted, depending on clay rock mineralogy, their content of organic matter and their texture, influenced by geological history.

4. Conclusion

Predictive approach and quantitative interpreting of gas adsorption by hydrated porous media is challenging, especially in case of such complex porous systems as clay minerals or clay rocks. This work aimed at better understanding the features of CH_4 and CO_2 adsorption

by clays saturated with water under controlled relative humidity conditions, assuming the mechanism of gas uptake by dissolution in clay water, as proposed earlier (Gadikota et al., 2017). The quantities of gases adsorbed per total amount of water in hydrated solids were directly compared with gas solubility in bulk water under the same (*P, T*) conditions. It was established that the solubility in water can reliably explain the CO_2 uptakes by hydrated porous media regardless of their nature. This observation is in line with relatively low "oversolubility" of CO_2 in nanoconfined liquids, as reported earlier (Pera-Titus et al., 2009; Rakotovao et al., 2010). The methane uptakes were properly described by dissolution as well, but only in case of solids with larger pores, where the confinement effects are not significant. On the other hand, in case of COx clay rocks, the adsorption-enhanced solubility of methane in pore water *vs.* bulk water (a ratio of 5-8) was observed, supposedly due to narrower pore sizes, in comparison to other systems, by analogy with SBA-15 silica. This finding potentially bears important consequences for industrial applications: both in case of shale gas behaviour and for radioactive waste disposal research: higher "solubility" of methane in the pore space of very compact clay-rocks should be better considered in performance assessment.

Acknowledgements

The present work was supported by the industrial chair "Storage and Disposal of Radioactive Waste" at IMT Atlantique, funded by ANDRA, Orano, and EDF.

References

AbdulKareem, F.A., Mohd. Shariff, A., Ullah, S., See, T.L., Keong, L.K., Mellon, N., 2018. Adsorption performance of 5A molecular sieve zeolite in water vapor–binary gas environment: Experimental and modeling evaluation. J. Ind. Eng. Chem. 64, 173–187. https://doi.org/10.1016/j.jiec.2018.03.014

Bardot, F., 1998. PhD Thesis: Surface heterogeneity of clay mineraIs: influence of surface compensating cations of illite on gas adsorption mechanisms 1–206.

Benoit, V., Chanut, N., Pillai, R.S., Benzaqui, M., Beurroies, I., Devautour-Vinot, S., Serre, C., Steunou, N., Maurin, G., Llewellyn, P.L., 2018. A promising metal-organic framework (MOF), MIL-96(Al), for CO2 separation under humid conditions. J. Mater. Chem. A 6, 2081–2090. https://doi.org/10.1039/c7ta09696h

Benson, S.M., Cole, D.R., 2008. CO2 sequestration in deep sedimentary formations. Elements 4, 325–331. https://doi.org/10.2113/gselements.4.5.325

Billemont, P., Coasne, B., De Weireld, G., 2013. Adsorption of carbon dioxide, methane, and their mixtures in porous carbons: Effect of surface chemistry, water content, and pore disorder. Langmuir 29, 3328–3338. https://doi.org/10.1021/la3048938

Billemont, P., Coasne, B., De Weireld, G., 2011. An experimental and molecular simulation study of the adsorption of carbon dioxide and methane in nanoporous carbons in the presence of water. Langmuir 27, 1015–1024. https://doi.org/10.1021/la103107t

Botan, A., Rotenberg, B., Marry, V., Turq, P., Noetinger, B., 2010. Carbon Dioxide in Montmorillonite Clay Hydrates: Thermodynamics, Structure, and Transport from Molecular Simulation. J. Phys. Chem. C 114, 14962–14969. https://doi.org/10.1021/jp1043305

Bowers, G.M., Loring, J.S., Schaef, H.T., Walter, E.D., Burton, S.D., Hoyt, D.W., Cunniff, S.S., Loganathan, N., Kirkpatrick, R.J., 2018. Interaction of Hydrocarbons with Clays under Reservoir Conditions: In Situ Infrared and Nuclear Magnetic Resonance Spectroscopy and X-ray Diffraction for Expandable Clays with Variably Wet Supercritical Methane. ACS Earth Sp. Chem. 2, 640–652. https://doi.org/10.1021/acsearthspacechem.8b00039

514 Bowers, G.M., Loring, J.S., Walter, E.D., Burton, S.D., Bowden, M.E., Hoyt, D.W., Arey, B.,
515 Larsen, R.K., Kirkpatrick, R.J., 2019. Influence of Smectite Structure and Hydration on
516 Supercritical Methane Binding and Dynamics in Smectite Pores. J. Phys. Chem. C 123,
517 29231–29244. https://doi.org/10.1021/acs.jpcc.9b08875

518 Bowers, G.M., Todd Schaef, H., Loring, J.S., Hoyt, D.W., Burton, S.D., Walter, E.D.,
519 Kirkpatrick, J.R., 2017. Role of cations in CO2 adsorption, dynamics, and hydration in
520 smectite clays under in situ supercritical CO2 conditions. J. Phys. Chem. C 121, 577–
521 592. https://doi.org/10.1021/acs.jpcc.6b11542

522 Bradbury, M.H., Baeyens, B., 2009. Sorption modelling on illite Part I: Titration
523 measurements and the sorption of Ni, Co, Eu and Sn. Geochim. Cosmochim. Acta 73,
524 990–1003. https://doi.org/10.1016/j.gca.2008.11.017

525 Bratko, D., Luzar, A., 2008. Attractive surface force in the presence of dissolved gas: A
526 molecular approach. Langmuir 24, 1247–1253. https://doi.org/10.1021/la702328w

527 Busch, A., Alles, S., Gensterblum, Y., Prinz, D., Dewhurst, D.N., Raven, M.D., Stanjek, H.,
528 Krooss, B.M., 2008. Carbon dioxide storage potential of shales. Int. J. Greenh. Gas
529 Control 2, 297–308. https://doi.org/10.1016/j.ijggc.2008.03.003

530 Centineo, A., Nguyen, H.G.T., Espinal, L., Horn, J.C., Brandani, S., 2019. An experimental
531 and modelling study of water vapour adsorption on SBA-15. Microporous Mesoporous
532 Mater. 282, 53–72. https://doi.org/10.1016/j.micromeso.2019.03.018

533 Clauzier, S., Ho, L.N., Pera-Titus, M., Coasne, B., Farrusseng, D., 2012. Enhanced H 2
534 uptake in solvents confined in mesoporous metal-organic framework. J. Am. Chem. Soc.
535 134, 17369–17371. https://doi.org/10.1021/ja308157a

536 Coasne, B., Farrusseng, D., 2019. Gas oversolubility in nanoconfined liquids: Review and
537 perspectives for adsorbent design. Microporous Mesoporous Mater. 288, 109561.

538 https://doi.org/10.1016/j.micromeso.2019.109561

539 Cooper, J., Stamford, L., Azapagic, A., 2016. Shale Gas: A Review of the Economic,
540 Environmental, and Social Sustainability. Energy Technol. 4, 772–792.
541 https://doi.org/10.1002/ente.201500464

542 Cychosz, K.A., Guillet-Nicolas, R., García-Martínez, J., Thommes, M., 2017. Recent
543 advances in the textural characterization of hierarchically structured nanoporous
544 materials. Chem. Soc. Rev. 46, 389–414. https://doi.org/10.1039/c6cs00391e

545 Diamond, L.W., Akinfiev, N.N., 2003. Solubility of CO2 in water from -1.5 to 100°C and
546 from 0.1 to 100 MPa: Evaluation of literature data and thermodynamic modelling. Fluid
547 Phase Equilib. 208, 265–290. https://doi.org/10.1016/S0378-3812(03)00041-4

548 Du, X., Guang, W., Cheng, Y., Hou, Z., Liu, Z., Yin, H., Huo, L., Lei, R., Shu, C., 2020.
549 Thermodynamics analysis of the adsorption of CH4 and CO2 on montmorillonite. Appl.
550 Clay Sci. 192, 105631. https://doi.org/10.1016/j.clay.2020.105631

551 Duan, Z., Mao, S., 2006. A thermodynamic model for calculating methane solubility, density
552 and gas phase composition of methane-bearing aqueous fluids from 273 to 523 K and
553 from 1 to 2000 bar. Geochim. Cosmochim. Acta 70, 3369–3386.
554 https://doi.org/10.1016/j.gca.2006.03.018

555 Feng, D., Li, X., Wang, X., Li, J., Sun, F., Sun, Z., Zhang, T., Li, P., Chen, Y., Zhang, X.,
556 2018a. Water adsorption and its impact on the pore structure characteristics of shale clay.
557 Appl. Clay Sci. 155, 126–138. https://doi.org/10.1016/j.clay.2018.01.017

558 Feng, D., Li, X., Wang, X., Li, J., Sun, F., Sun, Z., Zhang, T., Li, P., Chen, Y., Zhang, X.,
559 2018b. Water adsorption and its impact on the pore structure characteristics of shale clay.
560 Appl. Clay Sci. 155, 126–138. https://doi.org/10.1016/j.clay.2018.01.017

561 Ferrage, E., 2016. Investigation of the interlayer organization of water and ions in smectite

562 from the combined use of diffraction experiments and molecular simulations. A review
563 of methodology, applications, and perspectives. Clays Clay Miner. 64, 348–373.
564 https://doi.org/10.1346/CCMN.2016.0640401

565 Ferrage, E., Lanson, B., Michot, L.J., Robert, J.L., 2010. Hydration properties and interlayer
566 organization of water and ions in synthetic na-smectite with tetrahedral layer charge. Part
567 1. Results from X-ray diffraction profile modeling. J. Phys. Chem. C 114, 4515–4526.
568 https://doi.org/10.1021/jp909860p

569 Gaboreau, S., Robinet, J.C., Prêt, D., 2016. Optimization of pore-network characterization of
570 a compacted clay material by TEM and FIB/SEM imaging. Microporous Mesoporous
571 Mater. 224, 116–128. https://doi.org/10.1016/j.micromeso.2015.11.035

572 Gadikota, G., Dazas, B., Rother, G., Cheshire, M.C., Bourg, I.C., 2017. Hydrophobic
573 Solvation of Gases (CO2, CH4, H2, Noble Gases) in Clay Interlayer Nanopores. J. Phys.
574 Chem. C 121, 26539–26550. https://doi.org/10.1021/acs.jpcc.7b09768

575 Gaucher, E., Robelin, C., Matray, J.M., Négrel, G., Gros, Y., Heitz, J.F., Vinsot, A., Rebours,
576 H., Cassagnabère, A., Bouchet, A., 2004. ANDRA underground research laboratory:
577 Interpretation of the mineralogical and geochemical data acquired in the Callovian-
578 Oxfordian formation by investigative drilling. Phys. Chem. Earth 29, 55–77.
579 https://doi.org/10.1016/j.pce.2003.11.006

580 Gaucher, É.C., Blanc, P., Bardot, F., Braibant, G., Buschaert, S., Crouzet, C., Gautier, A.,
581 Girard, J.P., Jacquot, E., Lassin, A., Negrel, G., Tournassat, C., Vinsot, A., Altmann, S.,
582 2006. Modelling the porewater chemistry of the Callovian-Oxfordian formation at a
583 regional scale. Comptes Rendus - Geosci. 338, 917–930.
584 https://doi.org/10.1016/j.crte.2006.06.002

585 Gensterblum, Y., Ghanizadeh, A., Cuss, R.J., Amann-Hildenbrand, A., Krooss, B.M.,

586 Clarkson, C.R., Harrington, J.F., Zoback, M.D., 2015. Gas transport and storage capacity
587 in shale gas reservoirs - A review. Part A: Transport processes. J. Unconv. Oil Gas
588 Resour. 12, 87–122. https://doi.org/10.1016/j.juogr.2015.08.001

589 Gensterblum, Y., Merkel, A., Busch, A., Krooss, B.M., 2013. High-pressure CH4 and CO2
590 sorption isotherms as a function of coal maturity and the influence of moisture. Int. J.
591 Coal Geol. 118, 45–57. https://doi.org/10.1016/j.coal.2013.07.024

592 Giesting, P., Guggenheim, S., Koster van Groos, A.F., Busch, A., 2012. Interaction of carbon
593 dioxide with Na-exchanged montmorillonite at pressures to 640bars: Implications for CO
594 2 sequestration. Int. J. Greenh. Gas Control 8, 73–81.
595 https://doi.org/10.1016/j.ijggc.2012.01.011

596 Grambow, B., 2016. Geological disposal of radioactive waste in Clay. Elements 12, 239–245.
597 https://doi.org/10.2113/gselements.12.4.239

598 Grekov, D., Montavon, G., Robinet, J.C., Grambow, B., 2019. Smectite fraction assessment in
599 complex natural clay rocks from interlayer water content determined by
600 thermogravimetric and thermoporometry analysis. J. Colloid Interface Sci. 555, 157–
601 165. https://doi.org/10.1016/j.jcis.2019.07.076

602 Grekov, D., Pré, P., Grambow, B., 2020. On the use of manometry method for measurement
603 of gas adsorption equilibria and characterization of clay texture with Derivative Isotherm
604 Summation. Appl. Clay Sci. 184, 105372. https://doi.org/10.1016/j.clay.2019.105372

605 Grekov, D.I., Kalinichev, A.G., Suzuki-Muresan, T., Pré, P., Grambow, B., 2021. Direct
606 Experimental Evidence of the Effects of Clay Particles' Basal-to-Lateral Surface Ratio
607 on Methane and Carbon Dioxide Adsorption. J. Phys. Chem. C 125, 11499–11507.
608 https://doi.org/10.1021/acs.jpcc.1c00039

609 Grekov, D.I., Suzuki-Muresan, T., Kalinichev, A.G., Pré, P., Grambow, B., 2020.

610 Thermodynamic data of adsorption reveal the entry of CH4 and CO2 in a smectite clay
611 interlayer. Phys. Chem. Chem. Phys. 22, 16727–16733.
612 https://doi.org/10.1039/d0cp02135k

613 Han, W., Li, A., Memon, A., Ma, M., 2021. Synergetic Effect of Water, Temperature, and
614 Pressure on Methane Adsorption in Shale Gas Reservoirs. ACS Omega.
615 https://doi.org/10.1021/acsomega.0c05490

616 Harrington, J.F., Horseman, S.T., 1999. Gas transport properties of clays and mudrocks. Geol.
617 Soc. Spec. Publ. 158, 107–124. https://doi.org/10.1144/GSL.SP.1999.158.01.09

618 Ho, L.N., Schuurman, Y., Farrusseng, D., Coasne, B., 2015. Solubility of Gases in Water
619 Confined in Nanoporous Materials: ZSM-5, MCM-41, and MIL-100. J. Phys. Chem. C
620 119, 21547–21554. https://doi.org/10.1021/acs.jpcc.5b06660

621 Holmboe, M., Wold, S., Jonsson, M., 2012. Porosity investigation of compacted bentonite
622 using XRD profile modeling. J. Contam. Hydrol. 128, 19–32.
623 https://doi.org/10.1016/j.jconhyd.2011.10.005

624 Hu, K., Mischo, H., 2020. Modeling High-Pressure Methane Adsorption on Shales with a
625 Simplified Local Density Model. ACS Omega 5, 5048–5060.
626 https://doi.org/10.1021/acsomega.9b03978

627 Hwang, J., Joss, L., Pini, R., 2019. Measuring and modelling supercritical adsorption of CO2
628 and CH4 on montmorillonite source clay. Microporous Mesoporous Mater. 273, 107–
629 121. https://doi.org/10.1016/j.micromeso.2018.06.050

630 Hwang, J., Pini, R., 2021. Enhanced Sorption of Supercritical CO 2 and CH 4 in the Hydrated
631 Interlayer Pores of Smectite. Langmuir 37, 3778–3788.
632 https://doi.org/10.1021/acs.langmuir.1c00375

633 Hwang, J., Pini, R., 2019. Supercritical CO2 and CH4 Uptake by Illite-Smectite Clay

634 Minerals. Environ. Sci. Technol. 53, 11588–11596.
635 https://doi.org/10.1021/acs.est.9b03638

636 Jeon, P.R., Choi, J., Yun, T.S., Lee, C.H., 2014. Sorption equilibrium and kinetics of CO2 on
637 clay minerals from subcritical to supercritical conditions: CO2 sequestration at nanoscale
638 interfaces. Chem. Eng. J. 255, 705–715. https://doi.org/10.1016/j.cej.2014.06.090

639 Kadoura, A., Narayanan Nair, A.K., Sun, S., 2016. Adsorption of carbon dioxide, methane,
640 and their mixture by montmorillonite in the presence of water. Microporous Mesoporous
641 Mater. 225, 331–341. https://doi.org/10.1016/j.micromeso.2016.01.010

642 Kamimura, Y., Endo, A., 2015. CO2 adsorption performance of mesoporous ceria with co-
643 adsorbed water. Chem. Lett. 44, 1494–1496. https://doi.org/10.1246/cl.150687

644 Klewiah, I., Berawala, D.S., Alexander Walker, H.C., Andersen, P., Nadeau, P.H., 2020.
645 Review of experimental sorption studies of CO2 and CH4 in shales. J. Nat. Gas Sci. Eng.
646 73, 103045. https://doi.org/10.1016/j.jngse.2019.103045

647 Kutarov, V. V., Schieferstein, E., 2019. Analytical equation for the mesopore size distribution
648 function of open cylindrical capillaries. Adsorpt. Sci. Technol. 37, 468–479.
649 https://doi.org/10.1177/0263617419846000

650 Li, J., Li, X., Wang, X., Li, Y., Wu, K., Shi, J., Yang, L., Feng, D., Zhang, T., Yu, P., 2016.
651 Water distribution characteristic and effect on methane adsorption capacity in shale clay.
652 Int. J. Coal Geol. 159, 135–154. https://doi.org/10.1016/j.coal.2016.03.012

653 Li, W., Nan, Y., You, Q., Jin, Z., 2020. CO2 solubility in brine in silica nanopores in relation
654 to geological CO2 sequestration in tight formations: Effect of salinity and pH. Chem.
655 Eng. J. 127626. https://doi.org/10.1016/j.cej.2020.127626

656 Li, W., Zhang, M., Nan, Y., Pang, W., Jin, Z., 2021. Molecular Dynamics Study on CO2
657 Storage in Water-Filled Kerogen Nanopores in Shale Reservoirs: Effects of Kerogen

658 Maturity and Pore Size. Langmuir 37, 542–552.
659 https://doi.org/10.1021/acs.langmuir.0c03232

660 Liang, L., Xiong, J., Liu, X., Luo, D., 2016. An investigation into the thermodynamic
661 characteristics of methane adsorption on different clay minerals. J. Nat. Gas Sci. Eng. 33,
662 1046–1055. https://doi.org/10.1016/j.jngse.2016.06.024

663 Lin, Y., Horita, J., Abe, O., 2018. Adsorption isotope effects of water on mesoporous silica
664 and alumina with implications for the land-vegetation-atmosphere system. Geochim.
665 Cosmochim. Acta 223, 520–536. https://doi.org/10.1016/j.gca.2017.12.021

666 Liu, C.C., Chou, H.J., Lin, C.Y., Janmanchi, D., Chung, P.W., Mou, C.Y., Yu, S.S.F., Chan,
667 S.I., 2020. The oversolubility of methane gas in nano-confined water in nanoporous
668 silica materials. Microporous Mesoporous Mater. 293, 109793.
669 https://doi.org/10.1016/j.micromeso.2019.109793

670 Liu, D., Yuan, P., Liu, H., Li, T., Tan, D., Yuan, W., He, H., 2013. High-pressure adsorption
671 of methane on montmorillonite, kaolinite and illite. Appl. Clay Sci. 85, 25–30.
672 https://doi.org/10.1016/j.clay.2013.09.009

673 Loganathan, N., Bowers, G.M., Yazaydin, A.O., Schaef, H.T., Loring, J.S., Kalinichev, A.G.,
674 Kirkpatrick, R.J., 2018. Clay Swelling in Dry Supercritical Carbon Dioxide: Effects of
675 Interlayer Cations on the Structure, Dynamics, and Energetics of CO2 Intercalation
676 Probed by XRD, NMR, and GCMD Simulations. J. Phys. Chem. C 122, 4391–4402.
677 https://doi.org/10.1021/acs.jpcc.7b12270

678 Loganathan, N., Yazaydin, A.O., Bowers, G.M., Kalinichev, A.G., Kirkpatrick, R.J., 2017.
679 Molecular dynamics study of CO2 and H2O intercalation in smectite clays: Effect of
680 temperature and pressure on interlayer structure and dynamics in hectorite. J. Phys.
681 Chem. C 121. https://doi.org/10.1021/acs.jpcc.7b06825

682 Loganathan, N., Yazaydin, A.O., Bowers, G.M., Ngouana-Wakou, B.F., Kalinichev, A.G.,
683 Kirkpatrick, R.J., 2020. Role of Cations in the Methane/Carbon Dioxide Partitioning in
684 Nano- And Mesopores of Illite Using Constant Reservoir Composition Molecular
685 Dynamics Simulation. J. Phys. Chem. C 124, 2490–2500.
686 https://doi.org/10.1021/acs.jpcc.9b10051

687 Loring, J.S., Ilton, E.S., Thompson, C.J., Martin, P.F., Rosso, K.M., Felmy, A.R., Schaef,
688 H.T., 2014. In Situ Study of CO2 and H2O Partitioning between Na − Montmorillonite
689 and Variably Wet Supercritical Carbon Dioxide. Langmuir 30, 6120–6128.
690 https://doi.org/10.1021/la500682t

691 Loring, J.S., Schaef, H.T., Turcu, R.V.F., Thompson, C.J., Miller, Q.R.S., Martin, P.F., Hu, J.,
692 Hoyt, D.W., Qafoku, O., Ilton, E.S., Felmy, A.R., Rosso, K.M., 2012. In situ molecular
693 spectroscopic evidence for CO2 intercalation into montmorillonite in supercritical carbon
694 dioxide. Langmuir 28, 7125–7128. https://doi.org/10.1021/la301136w

695 Luzar, A., Bratko, D., 2005. Gas solubility in hydrophobic confinement. J. Phys. Chem. B
696 109, 22545–22552. https://doi.org/10.1021/jp054545x

697 Maddox, M.W., Olivier, J.P., Gubbins, K.E., 1997. Characterization of MCM-41 using
698 molecular simulation: Heterogeneity effects. Langmuir 13, 1737–1745.
699 https://doi.org/10.1021/la961068o

700 Marschall, P., Horseman, S., Gimmi, T., 2005. Characterisation of gas transport properties of
701 the Opalinus Clay, a potential host rock formation for radioactive waste disposal. Oil Gas
702 Sci. Technol. 60, 121–139. https://doi.org/10.2516/ogst:2005008

703 Massat, L., Cuisinier, O., Bihannic, I., Claret, F., Pelletier, M., Masrouri, F., Gaboreau, S.,
704 2016. Swelling pressure development and inter-aggregate porosity evolution upon
705 hydration of a compacted swelling clay. Appl. Clay Sci. 124–125, 197–210.

https://doi.org/10.1016/j.clay.2016.01.002

Melnitchenko, A., Thompson, J.G., Volzone, C., Ortiga, J., 2000. Selective gas adsorption by metal exchanged amorphous kaolinite derivatives. Appl. Clay Sci. 17, 35–53. https://doi.org/10.1016/S0169-1317(00)00003-X

Merkel, A., Fink, R., Littke, R., 2016. High pressure methane sorption characteristics of lacustrine shales from the Midland Valley Basin, Scotland. Fuel 182, 361–372. https://doi.org/10.1016/j.fuel.2016.05.118

Merkel, A., Fink, R., Littke, R., 2015a. The role of pre-adsorbed water on methane sorption capacity of Bossier and Haynesville shales. Int. J. Coal Geol. 147–148, 1–8. https://doi.org/10.1016/j.coal.2015.06.003

Merkel, A., Gensterblum, Y., Krooss, B.M., Amann, A., 2015b. Competitive sorption of CH4, CO2 and H2O on natural coals of different rank. Int. J. Coal Geol. 150–151, 181–192. https://doi.org/10.1016/j.coal.2015.09.006

Myshakin, E.M., Saidi, W.A., Romanov, V.N., Cygan, R.T., Jordan, K.D., 2013. Molecular dynamics simulations of carbon dioxide intercalation in hydrated Na-montmorillonite. J. Phys. Chem. C 117, 11028–11039. https://doi.org/10.1021/jp312589s

Occelli, M.L., Olivier, J.P., Peridon-Melon, J.A., Auroux, A., 2002. Surface area, pore volume distribution, and acidity in mesoporous expanded clay catalysts from hybrid density functional theory (DFT) and adsorption microcalorimetry methods. Langmuir 18, 9816–9823. https://doi.org/10.1021/la020567o

Occelli, M.L., Olivier, J.P., Petre, A., Auroux, A., 2003. Determination of pore size distribution, surface area, and acidity in fluid cracking catalysts (FCCS) from nonlocal density functional theoretical models of adsorption and from microcalorimetry methods. J. Phys. Chem. B 107, 4128–4136. https://doi.org/10.1021/jp022242m

730 Parkhurst, D.L., Appelo, C. a. J., 2013. Description of Input and Examples for PHREEQC
731 Version 3 — A Computer Program for Speciation , Batch-Reaction , One-Dimensional
732 Transport , and Inverse Geochemical Calculations. U.S. Geological Survey Techniques
733 and Methods, book 6, chapter A43, 497 p., U.S. Geological Survey Techniques and
734 Methods, book 6, chapter A43.

735 Peng, C., Crawshaw, J.P., Maitland, G.C., Trusler, J.P.M., Vega-Maza, D., 2013. The pH of
736 CO2-saturated water at temperatures between 308 K and 423 K at pressures up to 15
737 MPa. J. Supercrit. Fluids 82, 129–137. https://doi.org/10.1016/j.supflu.2013.07.001

738 Pera-Titus, M., El-Chahal, R., Rakotovao, V., Daniel, C., Miachon, S., Dalmon, J.A., 2009.
739 Direct volumetric measurement of gas oversolubility in nanoliquids: Beyond Henry's
740 law. ChemPhysChem 10, 2082–2089. https://doi.org/10.1002/cphc.200900058

741 Pini, R., 2014. Assessing the adsorption properties of mudrocks for CO2 sequestration.
742 Energy Procedia 63, 5556–5561. https://doi.org/10.1016/j.egypro.2014.11.589

743 Plaat, H., 2009. Underground gas storage: Why and how. Geol. Soc. Spec. Publ. 313, 25–37.
744 https://doi.org/10.1144/SP313.4

745 Pozo, M., Pino, D., Bessieres, D., 2017. Effect of thermal events on maturation and methane
746 adsorption of Silurian black shales (Checa, Spain). Appl. Clay Sci. 136, 208–218.
747 https://doi.org/10.1016/j.clay.2016.11.026

748 Rakotovao, V., Ammar, R., Miachon, S., Pera-Titus, M., 2010. Influence of the
749 mesoconfining solid on gas oversolubility in nanoliquids. Chem. Phys. Lett. 485, 299–
750 303. https://doi.org/10.1016/j.cplett.2009.12.038

751 Rexer, T.F., Mathia, E.J., Aplin, A.C., Thomas, K.M., 2014. High-pressure methane
752 adsorption and characterization of pores in posidonia shales and isolated kerogens.
753 Energy and Fuels 28, 2886–2901. https://doi.org/10.1021/ef402466m

754 Robinet, J.C., Sardini, P., Coelho, D., Parneix, J.C., Prt, D., Sammartino, S., Boller, E.,
755 Altmann, S., 2012. Effects of mineral distribution at mesoscopic scale on solute diffusion
756 in a clay-rich rock: Example of the Callovo-Oxfordian mudstone (Bure, France). Water
757 Resour. Res. 48, 1–17. https://doi.org/10.1029/2011WR011352

758 Robinet, J.C., Sardini, P., Siitari-Kauppi, M., Prêt, D., Yven, B., 2015. Upscaling the porosity
759 of the Callovo-Oxfordian mudstone from the pore scale to the formation scale; insights
760 from the 3H-PMMA autoradiography technique and SEM BSE imaging. Sediment.
761 Geol. 321, 1–10. https://doi.org/10.1016/j.sedgeo.2015.02.007

762 Ross, D.J.K., Marc Bustin, R., 2009. The importance of shale composition and pore structure
763 upon gas storage potential of shale gas reservoirs. Mar. Pet. Geol. 26, 916–927.
764 https://doi.org/10.1016/j.marpetgeo.2008.06.004

765 Rother, G., Ilton, E.S., Wallacher, D., Hau, T., Schaef, H.T., Qafoku, O., Rosso, K.M., Felmy,
766 A.R., Krukowski, E.G., Stack, A.G., Grimm, N., Bodnar, R.J., 2013. CO2 sorption to
767 subsingle hydration layer montmorillonite clay studied by excess sorption and neutron
768 diffraction measurements. Environ. Sci. Technol. 47, 205–211.
769 https://doi.org/10.1021/es301382y

770 Schaef, H.T., Davidson, C.L., Owen, A.T., Miller, Q.R.S., Loring, J.S., Thompson, C.J.,
771 Bacon, D.H., Glezakou, V.A., McGrail, B.P., 2014. CO2 utilization and storage in shale
772 gas reservoirs: Experimental results and economic impacts. Energy Procedia 63, 7844–
773 7851. https://doi.org/10.1016/j.egypro.2014.11.819

774 Schaef, H.T., Ilton, E.S., Qafoku, O., Martin, P.F., Felmy, A.R., Rosso, K.M., 2012. In situ
775 XRD study of Ca 2+ saturated montmorillonite (STX-1) exposed to anhydrous and wet
776 supercritical carbon dioxide. Int. J. Greenh. Gas Control 6, 220–229.
777 https://doi.org/10.1016/j.ijggc.2011.11.001

778 Schaef, H.T., Loganathan, N., Bowers, G.M., Kirkpatrick, R.J., Yazaydin, A.O., Burton, S.D.,
779 Hoyt, D.W., Thanthiriwatte, K.S., Dixon, D.A., McGrail, B.P., Rosso, K.M., Ilton, E.S.,
780 Loring, J.S., 2017. Tipping Point for Expansion of Layered Aluminosilicates in Weakly
781 Polar Solvents: Supercritical CO2. ACS Appl. Mater. Interfaces 9, 36783–36791.
782 https://doi.org/10.1021/acsami.7b10590

783 Song, Y., Davy, C.A., Troadec, D., Blanchenet, A.M., Skoczylas, F., Talandier, J., Robinet,
784 J.C., 2015. Multi-scale pore structure of COx claystone: Towards the prediction of fluid
785 transport. Mar. Pet. Geol. 65, 63–82. https://doi.org/10.1016/j.marpetgeo.2015.04.004

786 Suzuki, S., Sato, H., Ishidera, T., Fujii, N., 2004. Study on anisotropy of effective diffusion
787 coefficient and activation energy for deuterated water in compacted sodium bentonite. J.
788 Contam. Hydrol. 68, 23–37. https://doi.org/10.1016/S0169-7722(03)00139-6

789 Thielemann, J.P., Girgsdies, F., Schlögl, R., Hess, C., 2011. Pore structure and surface area of
790 silica SBA-15: Influence of washing and scale-up. Beilstein J. Nanotechnol. 2, 110–118.
791 https://doi.org/10.3762/bjnano.2.13

792 Thommes, M., Kaneko, K., Neimark, A. V., Olivier, J.P., Rodriguez-Reinoso, F., Rouquerol,
793 J., Sing, K.S.W., 2015. Physisorption of gases, with special reference to the evaluation of
794 surface area and pore size distribution (IUPAC Technical Report). Pure Appl. Chem. 87,
795 1051–1069. https://doi.org/10.1515/pac-2014-1117

796 Tournassat, C., Gailhanou, H., Crouzet, C., Braibant, G., Gautier, A., Gaucher, E.C., 2009.
797 Cation Exchange Selectivity Coefficient Values on Smectite and Mixed-Layer
798 Illite/Smectite Minerals. Soil Sci. Soc. Am. J. 73, 928.
799 https://doi.org/10.2136/sssaj2008.0285

800 Tsujiguchi, T., Miyashita, Y., Osaka, Y., Kodama, A., 2016. Influence of contained water
801 vapor on performance of simulated biogas separation by pressure swing adsorption. J.

802 Chem. Eng. Japan 49, 251–256. https://doi.org/10.1252/jcej.14we283

803 Wang, H., Yin, Y., Bai, J., Wang, S., 2020. Multi-factor study of the effects of a trace amount
804 of water vapor on low concentration CO2 capture by 5A zeolite particles. RSC Adv. 10,
805 6503–6511. https://doi.org/10.1039/c9ra08334k

806 Wang, J., Wang, S., Xin, Q., Li, Y., 2017. Perspectives on water-facilitated CO2 capture
807 materials. J. Mater. Chem. A 5, 6794–6816. https://doi.org/10.1039/c7ta01297g

808 Yven, B., Sammartino, S., 2007. Mineralogy, texture and porosity of Callovo-Oxfordian
809 argillites of the Meuse/Haute-Marne region (eastern Paris Basin). Mémoires la Société
810 géologique Fr. 178, 73–90.

811 Zhao, J., Deng, S., Zhao, L., Yuan, X., Du, Z., Li, S., Chen, L., Wu, K., 2020. Understanding
812 the effect of H2O on CO2 adsorption capture: Mechanism explanation, quantitative
813 approach and application. Sustain. Energy Fuels 4, 5970–5986.
814 https://doi.org/10.1039/d0se01179g

815 Ziemiański, P.P., Derkowski, A., Szczurowski, J., Kozieł, M., 2020. The structural versus
816 textural control on the methane sorption capacity of clay minerals. Int. J. Coal Geol. 224,
817 103483. https://doi.org/10.1016/j.coal.2020.103483

818